ARL-TR-10206 ● SEP 2025

DEVCOM ARMY RESEARCH LABORATORY

Ultrafast Laser Shock Coupled with Spectroscopic Techniques: Tools in Investigations of the Initial Events of Shock-Induced Initiations

by Nhan C. Dang and Frank C. De Lucia Jr.

NOTICES

Disclaimers

The findings in this report are not to be construed as an official Department of the Army position unless so designated by other authorized documents.

Citation of manufacturer's or trade names does not constitute an official endorsement or approval of the use thereof.

Destroy this report when it is no longer needed. Do not return it to the originator.

ARL-TR-10206 ● SEP 2025

Ultrafast Laser Shock Coupled with Spectroscopic Techniques: Tools in Investigations of the Initial Events of Shock-Induced Initiations

Nhan C. Dang and Frank C. De Lucia Jr.
DEVCOM Army Research Laboratory

REPORT DOCUMENTATION PAGE

1. REPORT DATE	2. REPORT TYPE	3. DATES COVERED	
		START DATE	END DATE
September 2025	Technical Report	10/01/2024	8/30/2025

4. TITLE AND SUBTITLE
Ultrafast Laser Shock Coupled with Spectroscopic Techniques: Tools in Investigations of the Initial Events of Shock-Induced Initiations

5a. CONTRACT NUMBER	5b. GRANT NUMBER	5c. PROGRAM ELEMENT NUMBER
5d. PROJECT NUMBER	**5e. TASK NUMBER**	**5f. WORK UNIT NUMBER**

6. AUTHOR(S)
Nhan C. Dang and Frank C. De Lucia Jr.

7. PERFORMING ORGANIZATION NAME(S) AND ADDRESS(ES)
DEVCOM Army Research Laboratory
ATTN: FCDD-RLA-WA
Aberdeen Proving Ground, MD 21005

8. PERFORMING ORGANIZATION REPORT NUMBER
ARL-TR-10206

9. SPONSORING/MONITORING AGENCY NAME(S) AND ADDRESS(ES)	10. SPONSOR/MONITOR'S ACRONYM(S)	11. SPONSOR/MONITOR'S REPORT NUMBER(S)

12. DISTRIBUTION/AVAILABILITY STATEMENT
DISTRIBUTION STATEMENT A. Approved for public release: distribution unlimited.

13. SUPPLEMENTARY NOTES

14. ABSTRACT
The crucial steps in the predictive science of explosives occur in the first few hundreds of picoseconds during initiation. Experimental observations during this time frame will reveal essential information for modeling to enable the design of improved energetic molecules. Therefore, developing techniques to observe the dynamic responses of explosive molecules is necessary. In this report, we discuss the role of tabletop ultrafast laser shock coupled with ultrafast dynamic ellipsometry and transient absorption spectroscopy in exploring the dynamic responses of explosives during the picosecond time scale.

15. SUBJECT TERMS
ultrafast laser shock, ultrafast dynamic ellipsometry, indirect ultrafast laser heating, transient absorption, electronic excitation, Weapons Sciences

16. SECURITY CLASSIFICATION OF:			17. LIMITATION OF ABSTRACT	18. NUMBER OF PAGES
a. REPORT	b. ABSTRACT	C. THIS PAGE		
UNCLASSIFIED	UNCLASSIFIED	UNCLASSIFIED	UU	28

19a. NAME OF RESPONSIBLE PERSON	19b. PHONE NUMBER *(Include area code)*
Nhan C. Dang	(520) 691-6422

STANDARD FORM 298 (REV. 5/2020)
Prescribed by ANSI Std. Z39.18

Contents

List of Figures

List of Tables

1. Introduction

Predicting performance and sensitivity of an explosive requires understanding the initial events. Events include how and how fast the energies from shock wave and temperature jump (T-jump) are generated during shock loadings, and when and what reactions occur in the material since the impact. By having better insight into these factors, more powerful but stable explosives can be designed and produced. Therefore, development of both theoretical and experimental studies of the physical and chemical responses during initial impact are necessary.

At a molecular level, several theoretical studies were made to propose mechanisms for shock-induced initiations, but no consensus has been reached.[1–6] The thermal equilibrium hypothesis[1] proposes that all excitations and chemistry can be driven by a single temperature, while no electronic excitations are expected, and vibrations will be populated according to the Boltzmann distribution. The multiphonon up-pumping hypothesis[2] suggests that the delocalized shock wave preferentially excites low-frequency phonons, which must drive chemistry by anharmonic energy transfer to high-frequency vibrations. It also predicts that no electronic excitations are expected. Vibrational excitations will be athermal and time dependent. On the other hand, the mechano-chemistry hypothesis[4] describes that shock impacts directly excite the molecules. Bonds are compressed and bent, nuclear configuration changes rapidly, and electronic energy levels shift; thus, chemistry is dissimilar to chemistry under nonshock conditions. It predicts that electronic excitations or distortions of the electronic structure as well as vibrational excitations can be athermal and are expected to occur directly following the shock front.

Studies have also been made to validate the proposed mechanisms described above by observing material responses under shock loadings at the time and length scales at the molecular level (i.e., picosecond time- and nanometer-length scales).[1–3,7–12] In those studies, one significant finding is that electronic excitations have been confirmed to be involved in ultrafast laser shock-induced reactions of materials in the time scale of approximately100 ps.[7–12] However, questions arose as to whether the changes are caused by shock-wave energy, thermal energy from T-jump during the shock loadings, or both. If thermal energy contributes to the changes, does it happen before or during the chemical reactions? A further attempt was recently made to observe the time evolution of chemistry in shocked materials by monitoring bond specifics of benzene and nitromethane using mid-infrared transient absorption spectroscopy.[11] In that study, the influences of temperature and shock pressure on specific chemical bonds were also investigated by monitoring spectral broadenings and shifts of these bonds during shock loadings. This strongly suggests the involvement of temperature during the initial events of shock-induced

initiation. To obtain a more complete understanding, further investigations of the time evolution of the T-jump roles/functions are still needed to fully describe the mechanisms of shock-induced initiations.

To experimentally validate the hypotheses and address these questions, we have been systematically establishing experimental capabilities to investigate how explosives will react during the initial events on the time and length scales of the molecular responses. Three experimental systems have been implemented at the U.S. Army Combat Capabilities Development Command (DEVCOM) Army Research Laboratory (ARL) to investigate the role(s)/function(s) of optical pump,[13] T-jump,[14–17] and shock stress in the initial events of explosive initiations. An optical pump-probed technique has been used to investigate electronic excitations of explosives under optical pump. The results obtained serve as standard electronic excitations that are then compared to those observed under heat and shock loadings. Consequentially, the comparisons reveal the role(s) of electronic excitations in shock-induced initiations. In the indirect ultrafast laser heating technique, a T-jump generation analogous to that generated during a shock event, coupled with transient absorption spectroscopies, has been used to investigate the role(s)/function(s) of T-jump in the changes of explosive electronic configurations. Obtained results will be compared to those obtained in shock-induced initiation studies. Knowledge gained from the comparisons will elucidate mechanisms and the role(s) of electronic excitations in shock-induced initiations.

In this report we describe and discuss the capabilities of investigating the physics and chemistries of explosives in the initial events (i.e., the first 350 ps) using an ultrafast laser shock technique coupled with ultrafast dynamic ellipsometry (UDE) and transient absorption (TA) spectroscopy to measure shock states and electronic excitations of explosives.

2. Techniques

2.1 Laser System

The laser system used in the ultrafast laser shock experiments is a commercial Ti:sapphire two-stage amplified chirped pulse system centered at 800 nm and operated at a repetition rate of 10 Hz. The first stage of the laser pulse amplification is the regeneratively amplified stage of a femtosecond laser system (Hydra, Coherent), which is summarized in Figure 1. In this stage, first, the input pulse is temporally stretched out using a dispersive delay line (stretcher), then amplified to saturation with a high-power solid-state laser, which gives a pulse energy of 1 mJ. In the second stage of the laser pulse amplification, the regeneratively amplified

stage of the femtosecond laser system is then amplified further with a 300-mJ YAG-Nd laser (Precision II 8000, Continuum Electro-Optics) to provide a total energy output up to 20 mJ for the system. The laser pulse at this step is called a "chirped pulse" in which laser frequencies are stretched out in time (i.e., the light for each laser frequency arrives at a different time). To create a shock wave that closely resembles the temporal shape of shock waves generated by the impact of a projectile, the intensity of the laser pulse is temporally shaped to yield a supported shock wave with a sharp (short rise time) shock front. Then, in the chirped pulse path, a razor edge is inserted into the low-frequency (temporally leading) side of the spectrum at the Fourier plane in the postamplification stretcher to remove the long wavelength parts of the spectrum (Figure 2) and impose a sharp rise time (5 ps) on the leading edge of the 300-ps full-width at half-maximum (FWHM) chirped pulse. The spectrally shaped chirped pulse is split into 80:20 by an 80:20 beam splitter. The 80% chirped pulse is directed for shock generation and UDE probes, while the 20% pulse is then recompressed using an inverse delay line (compressor) to obtain a compressed laser pulse of approximately 100 fs and directed for spectroscopic probing material responses under shock loadings.

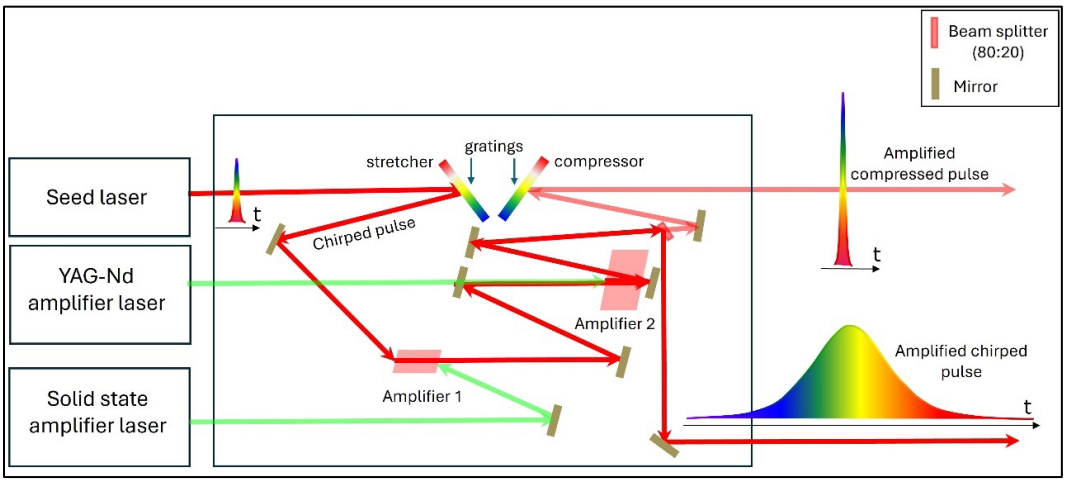

Figure 1. Schematic diagrams of the two-stage amplified chirped pulse of a femtosecond laser system.

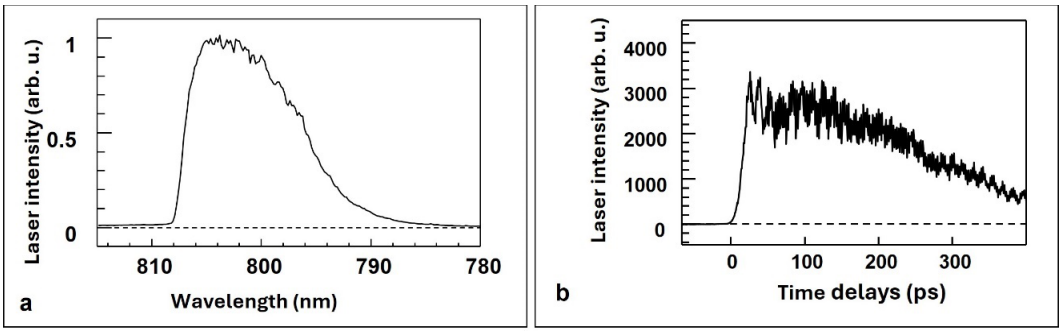

Figure 2. a) Spectrally shaped chirped laser spectrum, which is sharply cut in the lower frequencies to generate sharp rise of the heat pulse. b) Map-out of laser intensities of different wavelengths as a function of time.

2.2 Shock Generation

As shown in Figure 3, the spectrally shaped chirped pulse from one of the laser system outputs is directed and split into shock drive and UDE probe pulses with another 80:20 beam slitter. Then, 80% of the pulse is directed for shock generation and focused onto the 2-μm aluminum (Al) film (vapor deposited on a 500-μm-thick sapphire substrate) with a spot size of 65 μm. During laser ablation on the Al film, shock waves are generated in the Al film, where the laser energy heated the electrons in Al, and the hot electrons travel ballistically through the cold metal lattice to approximately the electron–phonon coupling length of the metal. The thermal energy in the electrons is coupled into the metal lattice via electron–phonon interactions, heating the metal lattice, which expands in response to the temperature jump to create the shock wave throughout the metal onto the sample deposited on the Al film. Note that the sapphire substrate acts as a tamper to prevent rapid expansion of the material back toward the laser drive pulse and to force the expansion into the metal film.

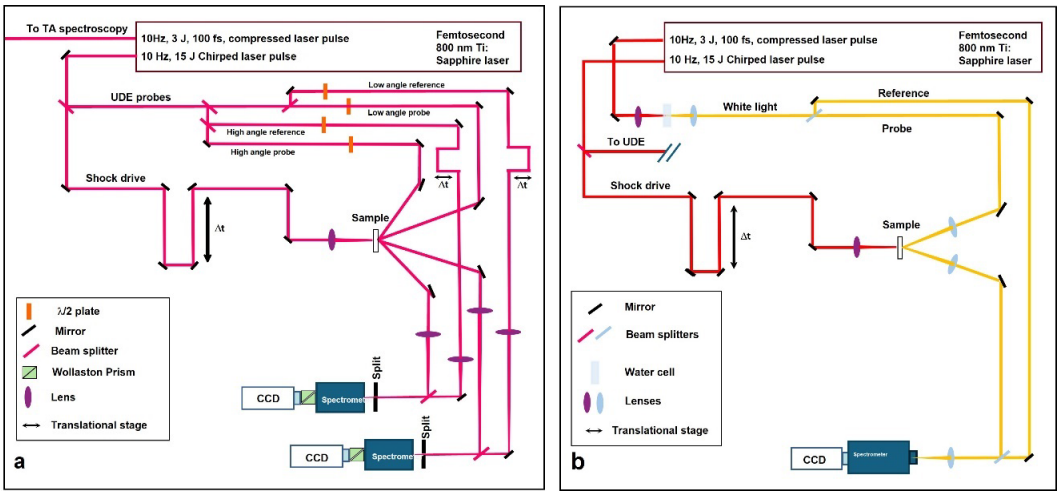

Figure 3. Schematic diagrams for experiments: a) ultrafast laser shock coupled with UDE and b) ultrafast laser shock coupled with visible (VIS) TA spectroscopy.

2.3 Ultrafast Dynamic Ellipsometry

The ultrafast laser shock coupled with UDE technique was well documented in previous studies.[18,19] In this report, a brief description and technical notes of UDE fundamentals are described.

The scheme of the ultrafast laser shock coupled with UDE and TA used to probe material responses under shock loadings in picosecond time scale is also depicted in Figure 3. For the UDE probe, the 20% spectrally shaped chirped pulse (after split from the shock drive pulse) is employed to UDE probes (Figure 3a), while the compressed pulse (directly out of the laser) is used for probing TA of shocked materials (Figure 3b). In Figure 3a, for shock generation, the chirped and spectrally shaped pulse is focused through a 150-mm focal length lens on the back side of Al–sapphire substrate; and 20% of the laser pulse from the chirped pulse is split off and equally split into two Mach–Zehnder interferometers that probe the sample at two different angles: 30° (low angle) and 63° (high angle) from normal. Both probes illuminate the same region of the sample area where the shock breakout occurs. In each arm of each interferometer, before the sample a halfwave plate is inserted. It is rotated such that S- and P-polarized light have equal intensities at the detectors after the spectrometers. The sample surface is then imaged with achromatic doublet lenses onto the entrance slits of the two imaging spectrometers, one for each angle. Identical lenses in the reference arms balanced the interferometers. The reference and probe beams are temporally and spatially crossed at a slight angle on the slits of the spectrometers, creating interference fringes perpendicular to the spectrometer slit. At the output of each spectrometer, a Wollaston prism separated the orthogonal polarizations into separate images on

charge-coupled device (CCD) cameras. Figure 4 shows interferograms recorded before and during a shock in a 7-μm spin-coated film of pentaerythritol tetranitrate (PETN).

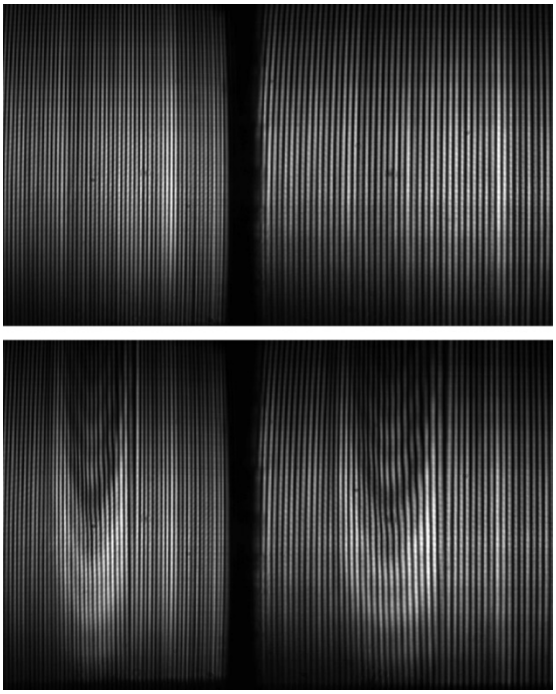

Figure 4. Interferograms of the 30° probe with the P-polarized light on the right and the S-polarized light on the left recorded before and during a 20-GPa shock in 7 μm of PETN on 2 μm of Al. The ripples observed during shock loading are indicative of surface motions or changes in the optical properties of the sample.

To measure the time-dependent intensity of the chirped pulse, a cross-correlation frequency-resolved optical gating (XFROG)[20] method is used. The portion of the 10-Hz pulse that is compressed was spectrally narrowed to an FWHM bandwidth of 10 nm and compressed to approximately 100 fs. This compressed pulse is combined with the chirped pulse in a 1-mm-thick Type I b-barium borate (BBO) crystal to generate the sum frequency of the two pulses. Data from the XFROG is shown in Figure 5. The calibrated spectrometers combined with the measured XFROG are used to interpolate the interferograms onto an evenly spaced time grid. The interferograms are then inversed via fast Fourier transform (FFT) along the spatial axis to give the phase shifts of the probe pulse and the reflectivity. Fitting the phase shifts and reflectivity data to shock simulations provides the particle velocity, u_p, and the shock velocity, u_s. In this report, the Levenberg–Marquardt least squares fitting algorithm is used. Note that, for Al, the measurement of the reflected light from a bare Al surface as a shock wave emerges yields a phase shift that is primarily a result of the movement of the free surface; therefore, the free-

surface velocity is analogous to u_p in this case. However, for thin film samples on an Al surface, the phase shift is primarily from the movement of the interface between the Al and the shocked samples, which results from the particle velocity of the sample; hence, the particle velocity u_p is used.

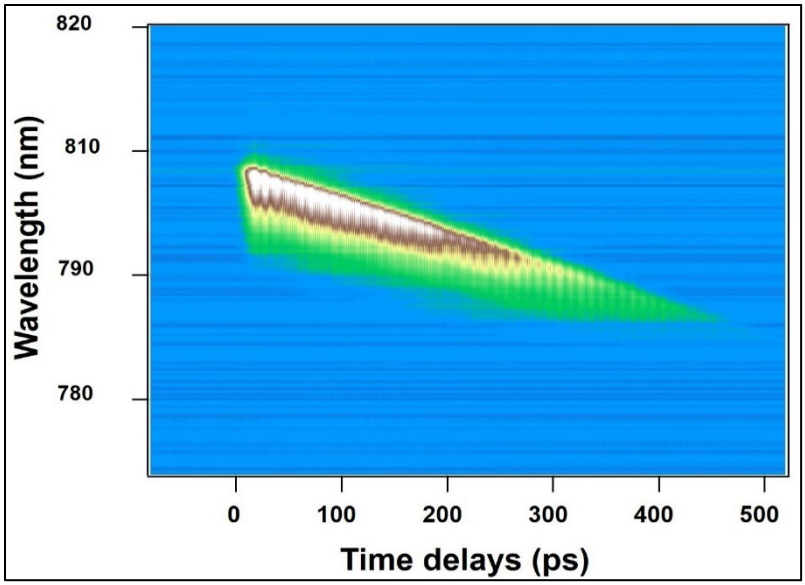

Figure 5. 2D scan of cross-correlation wavelength-resolved optical gating used to map out the laser wavelength in time.

2.4 Transient Absorption Measurements

Figure 3b shows the TA experimental scheme coupled with the ultrafast laser shock technique. In this figure, the compressed laser pulse centered at approximately 800 nm with a pulse width of approximately 100 fs is directed through a 75-mm focal length lens and focused on the center of a 1-cm water cell to generate a white light (WL) supercontinuum. To obtain a stable WL spectrum, the beam size, focal length, and energy of the input 800-nm laser beam are optimized such that nonlinear interactions within the water cell are minimal. The WL is then re-collimated with a 150-mm focal length lens. The beam is further spatially filtered by an iris to obtain the most stable and intense WL. The WL is then split into probe and reference beams via 50:50 beamsplitter. The probe beam is focused on the sample using a 200-mm focal length lens with an external angle of incidence of 30° and a spot size of 20 μm. The reflected probe is collimated with a 200-mm focal length lens. The collimated probe and reference pulses are then focused with a 75-mm focal length lens through a ground glass diffuser (ThorLabs DG10-1500) placed at the 100-μm slit of a home-built spectrometer. The diffuser removes spatial structure from the supercontinuum and allows normalized spectra to be acquired with a single shot standard deviation of 0.6%, despite significant (tens of percent peak-to-peak) shot-

to-shot spectral fluctuations. The spectrometer resolution is 2.5 nm and covers the range 380–780 nm. A thermoelectrically cooled, electronically gated CCD detector (Teledyne, Retiga R6) recorded the sample and reference intensities on each shot using an integration over approximately 100 pixels for each spectral wavelength. Spreading the signal over 100 pixels in the nonspectrally resolved direction increased the effective dynamic range and signal-to-noise ratio.

The relative time between the supercontinuum and the shock arrival was determined by three steps. The first step is timing between UDE and supercontinuum pulses. This is done via pump-probe transient absorption in a 6-μm-thick silicon (Si) single crystal. The absorption edge of Si is sufficiently close to the pulse wavelengths at 800 nm to allow the UDE pulse to be used as a pump and the long wavelengths of the supercontinuum used as a probe. A photodiode with a filter blocking the 800-nm UDE scatter monitors the supercontinuum intensity while the time delay between the UDE and supercontinuum is scanned. The supercontinuum transmission drops when the sharply rising initial edge of the UDE pulse arrives. The relative time delay between the supercontinuum and the UDE pulse is determined within 10 ps. The second step is temporally calibrating the imaging spectrometers (i.e., measuring time-dependent of the chirp pulse). This step is done by measuring the chirp of the UDE pulse as described in Figure 5. The final step is determining the shock-wave arrival time on the images captured during shock loadings. The determination is done by identifying the onset of a UDE phase change indicated by a 0.2-rad phase shift in the UDE data due to the shock. The chirp of the UDE pulse (step 2) is measured with cross correlation of the second harmonic frequency resolved optical gating of the UDE pulse with a compressed pulse in a BBO crystal. In step 3, temporal overlaps of the supercontinuum, UDE, and shock arrival are determined at the onset of UDE phase changes greater than 0.2 rad observed in the UDE data due to the shock to make sure that shock waves begin entering the samples.

To measure TA, the percentage of the transient reflectance of probe pulses from the sample at various delay times relative to the shock pulse (i.e., as determined by the delay line position of the supercontinuum) is recorded with a time resolution of 50 ps and calculated by Equation 1:

$$R = \left[\frac{R_{shock}}{Reference} - \frac{R_{preshock}}{Reference}\right] \Big/ \frac{R_{preshock}}{Reference} \qquad (1)$$

where R_{shock} and $R_{preshock}$ are the reflectance recorded during and before shock loading, respectively. The probe intensity spectrum was normalized with respect to the reference for the same probe pulse to account for any fluctuations during measurements.

The absorbance was then calculated by Equation 2:

$$A = -\log(\mathrm{R} + 1), \tag{2}$$

Each time-resolved spectrum reported here is an average of five single-shot spectra recorded at five different sample spots at the same time delay.

2.5 Samples and Samples Configurations

Information for liquid samples used is provided in Table 1. Pure PETN was obtained from colleagues at ARL.

Table 1. Liquids, supplier and purity, density (ρ), refractive index (n), and sound speed (c).

Material	Supplier	ρ_0	n	c
Cyclohexane	Acros (99+%)	0.779	1.426	1.26
Benzene	Sigma Aldrich (99.5%)	0.874	1.501	1.31

Typical sample configurations for solids and liquids are shown in Figure 6. Starting from left to right, the layers for the solid samples (Figure 6a) are 500-µm sapphire substrate (Esco, not oriented), 2-µm Al film (vapor deposited on the back of the sapphire substrate), and approximately 5- to 10-µm-thick samples (deposited on the Au film surface using the spin-coating technique). For liquid samples (Figure 4b), the assembly (from left to right) consists of a 500-µm sapphire substrate (Esco, not oriented), 2-µm Al film (vapor deposited on the back of the sapphire substrate), approximately 50–100 µL of liquid sample pressed inside of a mylar spacer (Harrick Scientific: 25 µm), and a 500-µm sapphire window (Esco, not oriented). Except when otherwise specified, these sample configurations are used for each experiment.

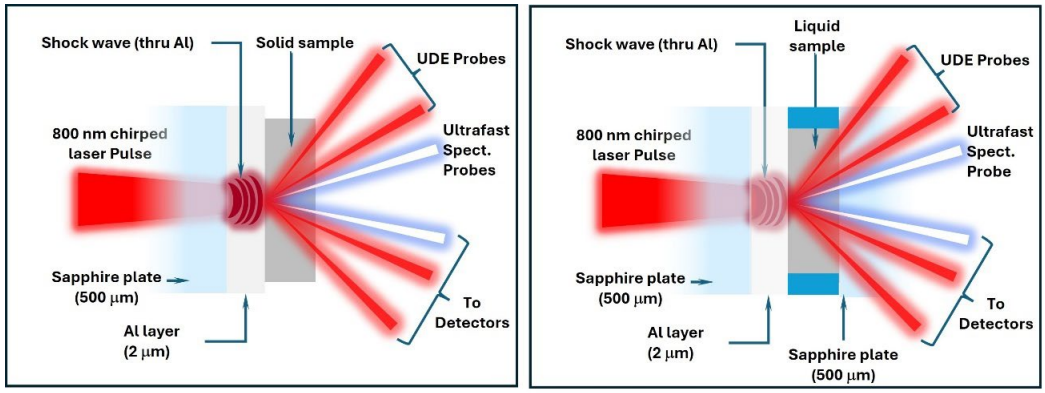

Figure 6. Schematic diagrams of sample configurations used in the experiments using the ultrafast indirect laser heating technique coupled with UV-VIS TA spectroscopy: a) configuration for solid sample and b) configuration for liquid sample.

3. Results and Discussion

3.1 Shock State of Thin Film Aluminum

Figure 7 represents UDE measurements and analysis of a shocked Al film with a laser energy of 3.0 mJ. Figure 7a shows an FFT image of the Al surface captured during shock loading for S- and P-polarization with a low-angle probe, while Figure 7b describes the phase shifts of both low- and high-angle probes for S- and P-polarization. The phase shift (blue) curves are taken from the Gaussian peaks over the shock region as indicated by the blue lines on the FFT image (Figure 7a). The simulation (red curves) is determined from the Levenburg–Marquardt best fit parameters. For clarification, the data and fits are offset horizontally from each other by 250 ps and displayed on the single time axis.

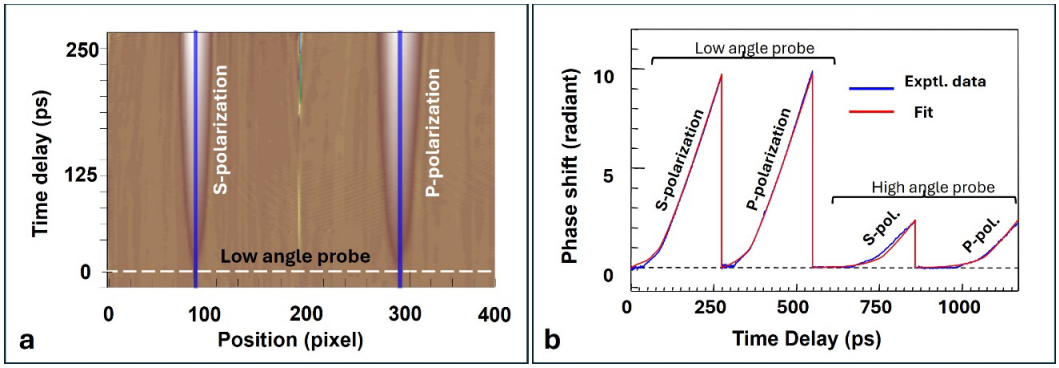

Figure 7. a) FFT image of the Al surface captured during shock loading for S- and P-polarization of the low-angle probe. b) Ultrafast dynamic ellipsometry data of shocked Al and fit to simulation (offset horizontally, from each other by 250 ps) for S- and P-polarization of both low- and high-angle probes. The data are lineouts from the center of the shocked region (as indicated by blue highlights in a).

Figure 8 shows Hugoniot of Al obtained from fitting the UDE at different laser energies and as previously reported in Marsh[21] (obtained from the traditional technique gas gun experiments). The agreement of the two datasets shown in Figure 8 confirm that the ultrafast laser shock coupled with the UDE technique offer the capability to accurately measure Hugoniots for thin film samples.

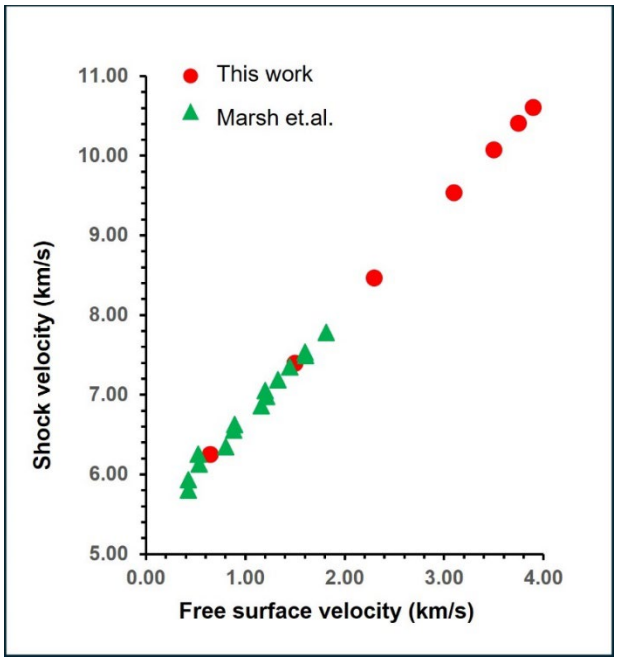

Figure 8. Shock and free surface/particle velocity of Al determined from the UDE fits plotted along with the traditional data by Marsh.[21]

3.2 Shock States and Observing Electronic Excitations of Thin Films of Cyclohexane, Benzene Liquids, and Solid Crystal PETN on 2-μm Al Films

To verify the experimental capability of observing electronic configuration changes of samples under shock loadings, cyclohexane was chosen as an inert sample, while benzene and PETN were selected as reactive liquid and solid samples, respectively. We expect to observe changes in the electronic configurations of benzene and PETN when perturbed by the shock stresses.

3.2.1 Inert Cyclohexane

Figure 9 represents UDE measurements and the analysis of the shocked cyclohexane with a shock stress of 18 GPa. Figure 9a is an FFT image of the cyclohexane surface captured during shock loading for S- and P-polarization, while Figure 9b shows shifts of both low- and high-angle probes for S- and P-polarization. The phase shift (blue) curves are taken from the Gaussian peaks over the shock region as indicated by the blue lines on the FFT image (Figure 9a). The simulation (red curves) is determined from the Levenburg–Marquardt best fit parameters. Note that, in thin film cyclohexane, oscillations in the phase shift are observed, which is different compared to the bare Al surface. These are from the thin film effects arising from the time-dependent thicknesses of the shocked and unshocked layers. Experimental u_p and u_s determined from the UDE fits and from previously reported

results[20] (obtained from the traditional technique-gas gun experiments) are illustrated in Figure 10. Compared to the two datasets in Figure 10, our UDE data match very well with the traditional data within the shock stress range that our experiment setup can generate.

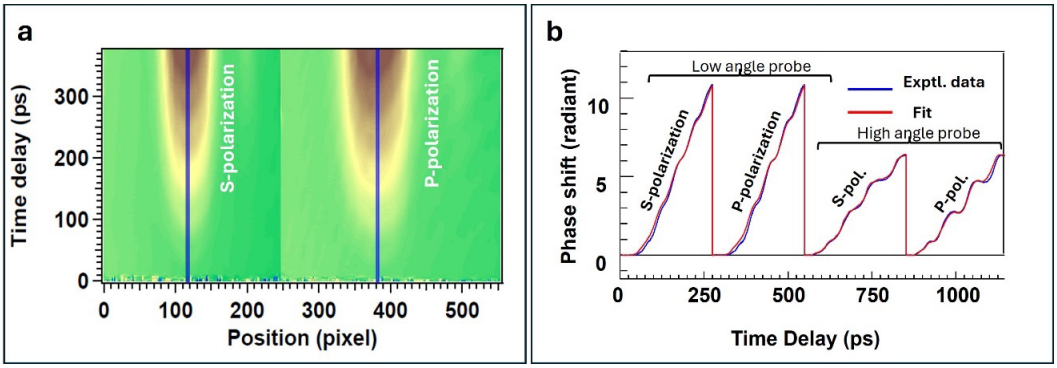

Figure 9. a) FFT image of a cyclohexane film on Al surface captured during shock loading for S- and P-polarization of the low-angle probe. b) Ultrafast dynamic ellipsometry data of shocked cyclohexane and fit to simulation (offset horizontally, from each other by 250 ps) for S- and P-polarization of both low- and high-angle probes. The data are lineouts from the center of the shocked region (as indicated in blue highlights in a).

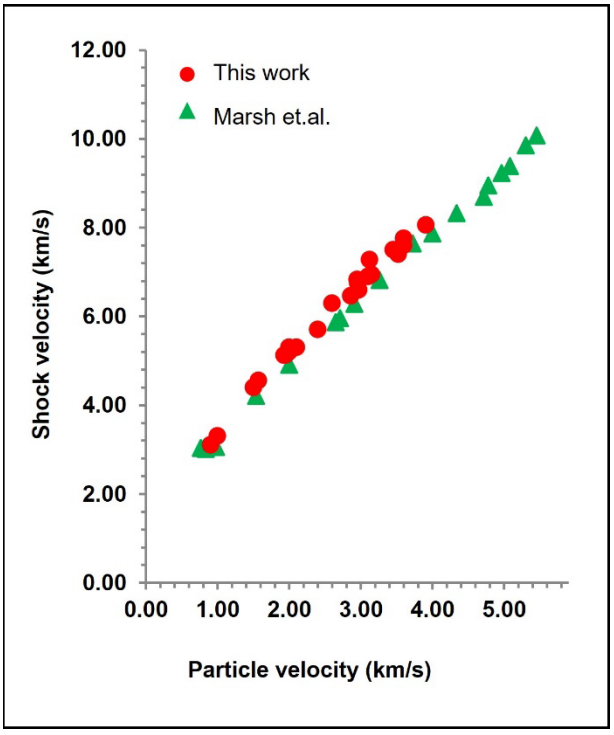

Figure 10. Shock and particle velocity of cyclohexane determined from the UDE fits are plotted along with the traditional data by Marsh.[21]

Figure 11 represents TA spectra of cyclohexane at two shock stresses: 5 GPa (upper panel) and 18 GPa (lower panel). As expected, cyclohexane exhibits a spectrally flat time-dependent absorption that grows with time delay after shock arrival. The observed absorption/reflectivity losses are due to the roughening of the Al surface and are defined here as the baseline level of the transient absorption spectra.

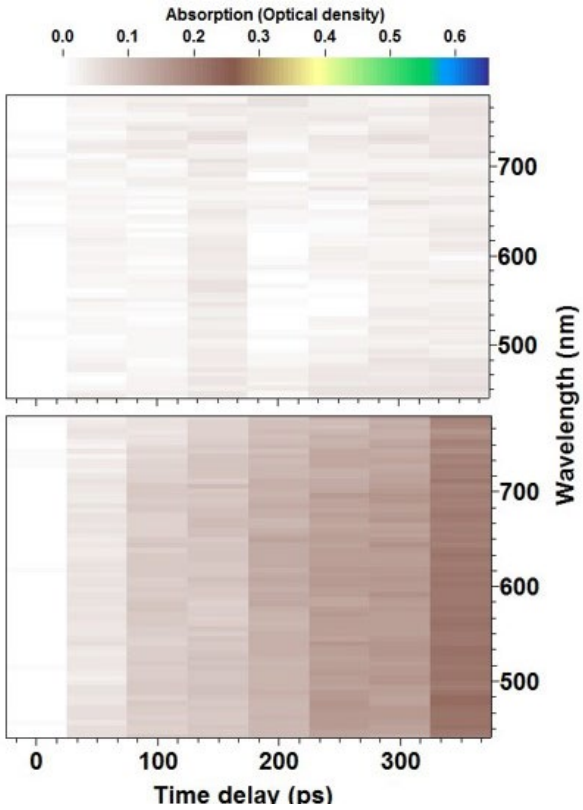

Figure 11. Transient absorption data are shown as a function of wavelength and time delay after shock arrival at the Al/liquid interface for cyclohexane with shock stresses of 5 GPa (upper panel) and 18 GPa (lower panel).

3.2.2 Reactive Transparent Liquid Benzene

Figure 12 shows Hugoniots for benzene in which experimental u_p and u_s determined from the UDE fits and previously reported results obtained from traditional methods.[20] In this figure, the liquid benzene obtained with UDE matches the data obtained with traditional techniques at u_p below 2.8 km/s. However, above 2.8 km/s both data start to deviate from the linear trend. The appearance of a kink in the Hugoniot is indicative of a chemical reaction leading to a higher-density product, signaling the beginning of chemical reactions. Note that the appearance of the kink in the Hugoniot in our experiments appears at higher shock stress than reported in the traditional experiments, which are sensitive to longer time scales (as shown in Figure 12). This suggests that the measured u_p and u_s can become interwoven with the chemical reaction dynamics in a manner that is sensitive to the degree of

reaction relative to the time window of the measurement. Reactions that proceed on hundreds of nanosecond time scales (e.g., at 5 GPa), will appear nonreactive in 350 ps. These reactions become apparent at 350 ps when they are sufficiently overdriven and the rate increases. Thus, we should expect to see different apparent "reaction thresholds" when the observation time window changes by orders of magnitude.

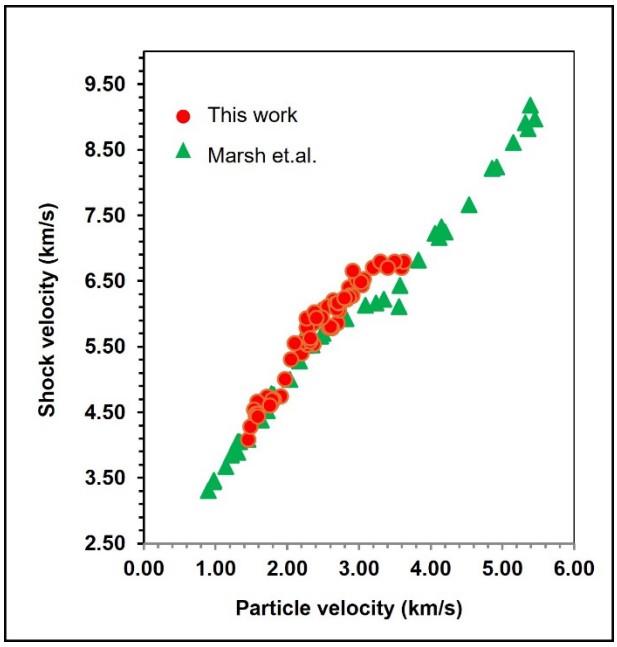

Figure 12. Shock and particle velocity of benzene determined from the UDE fits are plotted along with the traditional data by Marsh.[21]

Figure 13 depicts TA spectra of benzene as a function of time delay at two shock stresses of 7 and 20 GPa. As observed in Figure 12, at the shock stress of 20 GPa, TA of benzene starts approximately 100 ps after shock arrival at the Al/benzene interface. Note that for the traditional data shown in Figure 12, benzene was observed to undergo volume-decreasing reactions when shocked above 14 GPa on the time scales hundreds of nanoseconds to microseconds; however, data in this work show similar effects at over 20 GPa but occur approximately 3 orders of magnitude faster.

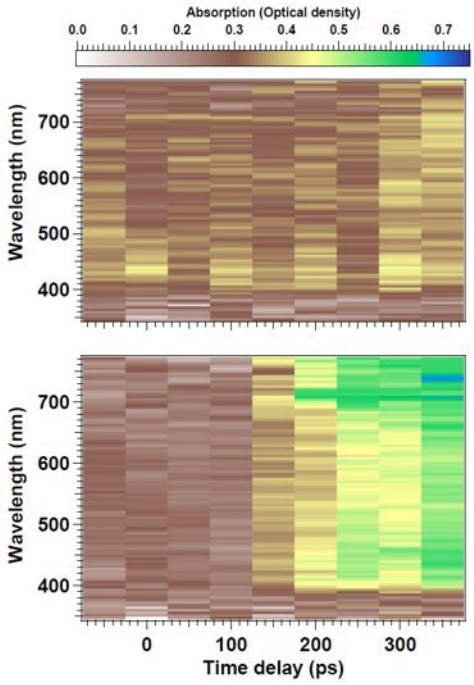

Figure 13. Transient absorption data are shown as a function of wavelength and time delay after shock arrival at the Al/liquid interface for benzene with shock stresses of 5 GPa (upper panel) and 20 GPa (lower panel).

3.3 Semi-Transparent Solid PETN

Figure 14 represents UDE measurements and analyses of the shocked PETN with a shock stress of 17 GPa. Figure 14a is an FFT image of the cyclohexane surface captured during shock loading for S- and P-polarization, while Figure 14b shows the phase shifts of the probes indicated by blue lines at the peaks of the Gaussians of the shock regions (blue curve) along with the simulation (red curve) determined from the Levenburg–Marquardt best fit parameters. Similar to the thin liquid films, oscillations in the phase shifts are observed in PETN. However, in addition to the oscillations with the regular pattern, oscillations with much broader patterns appear at higher shock stresses, as denoted with asterisks in Figure 14b. We anticipate that for solid opaque samples under higher compression significantly stronger light scattering occurs in the opaque samples compared to that which occurs in transparent liquid samples. The scatter light is convoluted with the reflectance to give rise to the new broader oscillations. Due to this phenomenon, the models used for UDE fitting described by Bolme et al.[18,19] become inaccurate at higher shock stresses in solid samples. This can be seen in Figure 15 where experimental u_p and u_s determined from the UDE fits in this work along with traditional data reported in Marsh[21] and data obtained using a combination of UDE measurements and

impedance matching methods reported in Powell et al.[22] Compared to the two datasets in Figure 15, our UDE data match very well in the shock stress range below 1.5 km/s. Deviations become pronounced when u_s is faster than 1.5 km/s as can be seen in Figure 15 where the UDE Hugoniot trends above the data from Powell et al.[22] Therefore, for more accurate determinations of shock stresses in the opaque solid samples, the use of UDE measurements combined with impedance matching methods as discussed in Powell et al.[22] are necessary.

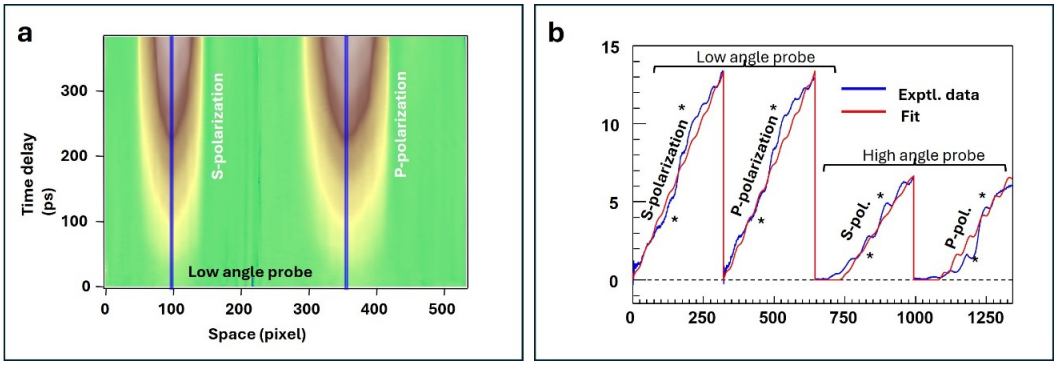

Figure 14. a) FFT image of 7-µm PETN film on Al surface captured during shock loading for S- and P-polarization of the low-angle probe. b) Ultrafast dynamic ellipsometry data of shocked PETN and fit to simulation (offset horizontally, from each other by 250 ps) for S- and P-polarization of both low- and high-angle probes. The data are lineouts from the center of the shocked region (as indicated in blue highlights in a).

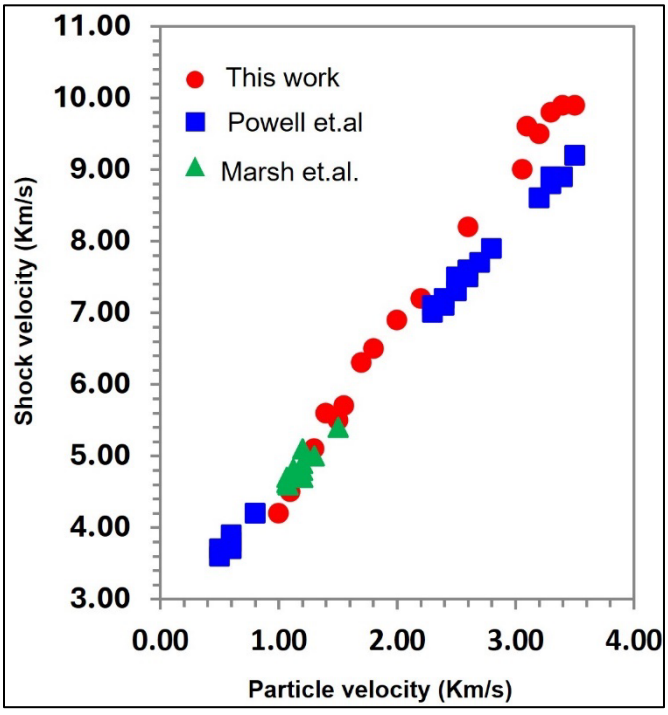

Figure 15. Shock and particle velocity of PETN determined from the UDE fits are plotted along with the data obtained using a combination of UDE and impedance matching by Powell et al.[22] and traditional data by Marsh.[21]

As shown in Figure 15, no indication of volume-decreasing reactions is observed in the shock stress range studied in this work. Using shock state in Al obtained with UDE measurements reported in Section 3.1, and impedance matching from reported Hugoniot of PETN[22,23] the maximum stress in the PETN obtained in this work is 23 GPa. Consistent with Hugoniot data, no TA was observed in the shock stress range in this study. To investigate PETN or other solid sample chemistry, higher shock stresses will be required. We are currently optimizing our system to obtain higher shock stress.

4. Conclusion

We have been building and developing state-of-the-art ultrafast experimental capabilities, essential tools for investigating the initial event of shock-induced initiation on the relevant picosecond time scale. The findings from these investigations combined with our ongoing investigations of explosives under optical pump and indirect ultrafast heating will provide essential knowledge to determine which key factors are involved in the initial events of shock-induced initiation. The goal is to experimentally determine mechanisms for shock-induced initiation, thus reducing the assumptions used in the modeling of predictive capabilities.

5. References

1. Dremin AN. Shock discontinuity zone effect – the main factor in the explosive decomposition detonation process. Phil Trans Royal Soc A. 1992;339:355–364.
2. Dlott DD, Fayer MD. Shocked molecular solids: vibrational up pumping, defect hot spot formation, and the onset of chemistry. J Chem Phys. 1990;92:3798–3812.
3. Gilman JJ. Mechanochemistry science. 1996;274:65–65.
4. Gilman JJ. Chemical-reactions at detonation fronts in solids. Phil Mag B. 1995;71:1057–1068.
5. Kuklja MM et al. Role of electronic excitations in explosive decomposition of solids. J Appl Phys. 2001;89:4156–4166.
6. Kunz AB, Kulja MM, Botcher TR, Russell TP. Initiation of chemistry in molecular solids by processes involving electronic excited states. Thermochimica Acta. 2002;384:279–284.
7. McGrane SD, Moore DS, Funk DJ. Shock induced reaction observed via ultrafast infrared absorption in poly(vinyl nitrate) films. J Phys Chem A. 2004;108(43):9342–9347.
8. Dang NC, Bolme CA, Moore DS, McGrane SD. Shock induced chemistry in liquids studied with ultrafast dynamic ellipsometry and visible transient absorption spectroscopy. J Phys Chem A. 2012;116(42):10301–10309.
9. Brown KE, Bolme CA, Moore DS, McGrane SD. Ultrafast chemical reactions in shocked nitromethane probed with dynamic ellipsometry and transient absorption spectroscopy. J Phys Chem A. 2014;118(14):2559–2567.
10. Brown KE, Bolme CA, Moore DS, McGrane SD. Ultrafast shock-induced chemistry in carbon disulfide probed with dynamic ellipsometry and transient absorption spectroscopy. J Appl Phys. 2015;117(8):085903.
11. Bowlan P et al. Probing ultrafast shock-induced chemistry in liquids using broad-band mid-infrared absorption spectroscopy. J Chem Phys. 2019;150(20):204503.
12. Powell MS et al. A benchtop shock physics laboratory: ultrafast laser driven shock spectroscopy and interferometry methods. Rev Sci Instrum. 2019;90(6):063001.

13. De Lucia FC Jr, Dang NC. Investigation of the role of electronic excitations in shock-induced initiations of explosives using an optical pump-probe technique. DEVCOM Army Research Laboratory (US); 2024 Sep. Report No.: ARL-TR-9968.

14. Dang NC, Gottfried JL, De Lucia FC Jr. Energetic material response to ultrafast indirect laser heating. Appl Opt. 2017;56(3):B85–B91.

15. Dang NC, Gottfried JL, De Lucia FC Jr. The initial response of energetic materials in the first 50 picoseconds. Proceedings for the 16th International Detonation Symposium; 2018.

16. Dang NC, Gottfried JL, De Lucia FC Jr. The responses of energetic materials under indirect ultrafast heating: polarization dependence of heat transfer in materials. DEVCOM Army Research Laboratory (US); 2023 Aug. Report No.: ARL-TR-9730.

17. Dang NC, Gottfried JL, De Lucia FC Jr. The electronic excitation of 2,4,6-triamino-1,3,5-trinitrobenzene in DMSO solution under indirect ultrafast heating: a comparison to results obtained by optical pumped method. DEVCOM Army Research Laboratory (US); 2023 Sep. Report No.: ARL-TR-9773.

18. Bolme CA, McGrane SD, Moore DS, Funk DJ. Single shock measurements of laser driven shock waves using ultrafast dynamic ellipsometery. J Appl Phys. 2007;102:033513.

19. Bolme CA, McGrane SD, Moore DS, Whitley VH, Funk DJ. Single shot Hugoniot of cyclohexane using a spatially resolved laser driven shock wave. Appl Phys Lett. 2008;93:191903.

20. Geindre JP, Audebert P, Rebibo S, Gauthier JC. Single-shot spectral interferometry with chirped pulses. Opt Lett. 2001;26:1612–1614.

21. Marsh SP. LASL shock Hugoniot data. University of California Press; 1980.

22. Powell MS et al. Insight into the chemistry of PETN under shock compression through ultrafast broadband mid-infrared absorption spectroscopy. J Phys Chem A. 2020;124:7031–7046.

23. Dick JJ. Shock response of pentaerythritol tetranitrate single crystals. J Appl Phys. 1991;70:3572–3587.

List of Symbols, Abbreviations, and Acronyms

2D	two-dimensional
Al	aluminum
ARL	Army Research Laboratory
BBO	b-barium borate
CCD	charge-coupled device
DEVCOM	U.S. Army Combat Capabilities Development Command
FFT	fast Fourier transform
FWHM	full-width at half-maximum
PETN	pentaerythritol tetranitrate
Si	silicon
TA	transient absorption
T-jump	temperature jump
UDE	ultrafast dynamic ellipsometry
UV	ultraviolet
VIS	visible
WL	white light
XFROG	cross-correlation frequency-resolved optical gating

1 (PDF)	DEFENSE TECHNICAL INFORMATION CTR DTIC OCA
1 (PDF)	DEVCOM ARL FCDD RLB CI TECH LIB